Journal of Science and Technology – Engineering and Technology for Sustainable Development
Volume 36, Issue 2, April 2026, 087–094

Strength Analysis of Horizontal-Axis Wind Turbine Blade

Hoang Thi Kim Dung*
Hanoi University of Science and Technology, Ha Noi, Vietnam
**Corresponding author email: dung.hoangthikim@hust.edu.vn*

Abstract

Wind energy is one of the forms of renewable energy that has been developed strongly in recent times. Wind turbines are used to take advantage of this free and clean energy source. To increase capacity, developers often increase the size of wind turbines. The increased size of the wind turbine leads to an increase in the size of the blades. Along with the increase in size, the deformation of the blade also increases as the blade size increases. The deformation that occurs during wind turbine operation is due to the pressure load distributed across the blades. Controlling the deformation of the turbine blade that occurs during operation will reduce the risk of cracking and breaking of the blade, thereby improving the performance of wind turbines, especially large sized wind turbines. In this paper, first Computational Fluid Dynamics (CFD) problem was solved to find the load distribution on the blade surface of GE1.5XLE turbine blade of horizontal-axis wind turbines (HAWT) with air velocity of 12 m/s. Then, this load distribution was used as an input condition for Fluid-Structure Interaction (FSI) problem to find out the deformation of the blade. The simulation methods using in this paper were estimated with help of ANSYS software. The results deviated by less than 2% from the manufacturer's data.

Keywords: ANSYS, CFD, FSI, HAWT, wind turbine.

1. Introduction

Renewable energy is being studied more and more due to the increase in energy demand, the depletion of fossil fuel resources, and environmental problems. Wind energy is one of the most rapidly developed forms of clean energy in recent times.

With the aim of increase the efficiency of the wind turbine as well as the amount of electricity it generates, the most advanced technologies have been studied with different aspects. One of those aspects is increasing the size of the wind turbine. This leads to the turbine blades becoming larger with more complex structures but still having to meet the material and cost requirements [1]. This tendency by manufacturers increases the risk of failure due to direct aeroelasticity phenomena such as dynamic stall, divergence, flutter, and load distribution [2]. These phenomena are the result of a combination of aerodynamic force, inertial force, and elastic force. Therefore, the study of the aeroelasticity of turbine blades is very important in the research and development of the next generation of wind turbines.

The history of using wind energy goes back thousands of years. At that time, it was used in sailing ships and for milling grain [3]. Vertical-axis wind rotors may have been used as early as 200 BC in the Sista region of Iran. Horizontal-axis windmills began to be used in Europe and the Mediterranean region between 1300 and 1875 AD [4]. The output power of the wind turbine must be converted to grid electricity or electrical loads. The output power also goes through other components such as wiring, transformers, etc. Normally, the output voltage of a wind turbine is up to 34.5 kilovolts. Offshore wind turbines often transmit electricity to the mainland by an undersea cable system [5].

Along with the history of evolution and development, modern wind turbines have been investigation and are classified into two types: horizontal-axis wind turbines (HAWT) and vertical-axis wind turbines (VAWT). In this paper, research of HAWT type is caried out as it has a more widely known design. A wind turbine consists of seven main components: rotor, drive strain, nacelle, generator, tower, and foundation, control system, and electrical output system [6, 7].

Viscous effects on wind turbine blades were investigated in [8]. In this report, dynamics stall decreased lift coefficient by the separation of flow on aerofoil as the angle of attack increases. This complex phenomenon requires consideration of many parameters such as transport flow, boundary layer, vortex generation, and separation of fluid flow as well as coefficient of friction in the boundary layer.

Hansen [9] researched on the stall-induced vibrations by analysing aeroelastic eigenvalues of a 3-blade turbine with a power of about MW. The limiting frequency of the first torsion had been calculated for which wing flapping occurred. Hansen remarked that the turbine dynamics also affect the risk of flutter. The critical torsional frequency was higher when the blades were

p-ISSN 3093-3242
e-ISSN 3093-3579
https://doi.org/10.51316/jst.189.etsd.2026.36.2.11
Received: Jan 23, 2025; Revised: Jun 27, 2025;
Accepted: Jun 30, 2025; Online: Mar 24, 2026

interacting through the hub with the remaining turbine, than when all blades were rigidly clamped at the root.

Recently, Mezaal *et al*. [10] performed analysis of new HAWT using Computational Fluid Dynamics (CFD) method with different aerofoil. The blade with a cylindrical shape at the root then transitions to the aerofoils S818, S825, and S826 for the root, body, and tip respectively. This blade was similar in size to a GE 1.5xle turbine by Cornell University.

Wang *et al* [11] established a one-way Fluid Structure Interaction (FSI) model for WindPACT 1.5 MW wind turbine blades at full scale. The CFD model implemented in ANSYS FLUENT, and the blade structural responses were determined using a Finite Element Analysis (FEA) model implemented in ANSYS Static Structural module. In the one-way coupling model, the aerodynamic loads calculated from CFD modelling were mapped to FEA model as load boundary conditions.

Shamso *et al*. [12] researched on a general Electric's HAWT for 1.5 MW of renewable energy and focused on using the ANSYS software to calculate the tip velocity, pressure, power coefficient, deflection, flap-wise, and edgewise deformation values with wind speeds from 7 to 20 m/s, blade position from 90º to 360º, and five composite materials of Carbon-Epoxy, E-Glass, S-Glass, Kevlar, and Technora.

Sakala *et al*. [13] carried out the performance analysis of the HAWT using CFD modeling, comparing with experimental data obtained from the wind turbine experiments carried out by Vermeer [14]. The 3D CFD calculations were done for the subsonic flow over a wind turbine rotor at various values of tip speed ratio and operating at a Reynolds number of 2x105 using Spalart – Allmaras, k-ω, and transitional SST turbulence models.

Vermeer [14] researched the measurement for verification of predictions with the theoretical model from Delft University in the Netherlands. The torque and axial force were measured for three configurations: blades without vanes, with v-vanes, and with s-vanes. For each of these configurations three pitch angles were set, and at one tunnel wind speed a rotational speed range has been considered.

Mamaghani and Jenkins [15] performed the aerodynamic characteristics of a multi-bladed HAWT rotor using the Shear Stress Transport (SST) *k*-ω turbulence model. Besides, the flow visualizations were done with four different wind velocities of 2.2, 4.5, 6.7, and 11 m/s.

The aim of this research is to carry out the load distribution and the deformation of the GE1.5XLE turbine blade of HAWT with air velocity of 12 m/s using ANSYS software. The model of blades is referred to Mezaal *et al*. [10].

2. Simulation Setup

2.1. Wind Turbine Blade Model

HAWT wind turbines included of three GE1.5XLE turbine blades. This turbine blade consisted of three different types of aerofoils S818, S825, and S826 with geometrical and technical parameters given in Mezaal *et al*. [10] (Fig. 1a). The blade profiles were designed along the blade from root to tip.

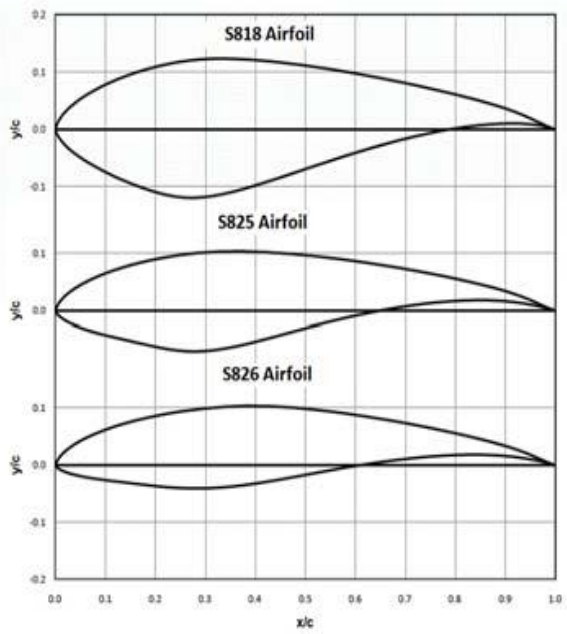

a. Airfoil

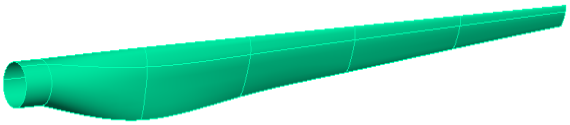

b. Blade model

Fig. 1. Wind turbine blade

The root of the blade started with cylindrical shaft. This shaft was transitioned to S818 profile, then S825 profile and finally S826 profile tip of the blade. Turbine blades were shown in Fig. 1b. Shape parameters of turbine blades, including twist, span, and chord length, were shown in Table 1.

This blade was designed for HAWT wind turbine with main parameters given in Table 2.

This blade was made by composite materials to reduce the mass of the blades and thereby significantly reduce the mass of the entire turbine. The property values of orthotropic composite materials in Table 3 were derived from the materials used to manufacture turbine blades in practice.

The aerodynamic and structural properties of this

blade were estimated by both CFD, FSI, and modal method with help of ANSYS software. Firstly, the CFD problem was solved to determine aerodynamic properties including pressure distribution (or aerodynamic loads) on the turbine blade. Secondly, the deformation caused by aerodynamic loads on turbine blades was estimated by solving one-way FSI problem.

Table 1. Geometric parameters of turbine blades

Span *(%)*	Span *(m)*	Twist *(°)*	Chord *(%)*	Chord *(m)*	Airfoil
0.075	3.094	42	0.061	2.533	
0.125	5.156	32	0.068	2.816	
0.175	7.219	23	0.075	3.074	
0.225	9.281	15	0.078	3.210	S818
0.275	11.344	11.5	0.075	3.112	
0.325	13.406	8.2	0.072	2.965	
0.375	15.469	7	0.068	2.818	
0.425	17.531	6	0.065	2.673	
0.475	19.594	5	0.061	2.527	
0.525	21.656	4	0.058	2.381	
0.575	23.719	4.15	0.054	2.234	
0.625	25.781	3.85	0.051	2.088	S825
0.675	27.844	3.25	0.047	1.942	
0.725	29.906	2.75	0.044	1.799	
0.775	31.969	1.25	0.040	1.660	
0.825	34.031	0.75	0.037	1.528	
0.875	36.094	0.55	0.034	1.396	
0.925	38.156	0.85	0.031	1.265	S826
0.975	40.219	0.05	0.027	1.133	
1	41.25	0	0.024	1	

Table 2. Main parameters of wind turbine

Parameter	Value	Unit
Rated power	1500	kW
Number of blades	3	-
Rotor diameter	86.5	m
Rated wind speed	12	m/s
Rotation speed	2.22	rad/s
Pitch angle	4	degree
Inlet air velocity	12	m/s

Table 3. Turbine blade material parameters

Parameter	**Value**
Density (kg/m^3)	1550
Young's Modulus-X (Pa)	1.1375E+11
Young's Modulus-Y (Pa)	7.583E+9
Young's Modulus-Z (Pa)	7.583E+9
Poisson's Ratio-XY	0.32
Poisson's Ratio-YZ	0.37
Poisson's Ratio-ZX	0.35
Shear Modulus-XY (Pa)	5.446E+9
Shear Modulus-YZ (Pa)	2.964E+9
Shear Modulus-ZX (Pa)	2.964E+9
Orthotropic Stress limits	
Tensile X direction (Pa)	1.98E+09
Tensile Y direction (Pa)	2.60E+07
Tensile Z direction (Pa)	2.60E+07
Compressive X direction (Pa)	8.93E+08
Compressive Y direction (Pa)	1.39E+07
Compressive Z direction (Pa)	1.39E+07
Shear XY (Pa)	1.00E+08
Shear YZ (Pa)	5.00E+07
Shear XZ (Pa)	1.00E+08

2.2. Computational Fluid Dynamics Setup

The governing equations of fluid flow are continuity equations and Navier-Stokes equations. These equations are written in a rotating frame of reference with the blades of the turbine. This has the important benefit of making the simulation not require a moving mesh to account for the rotation of the blades. These equations are reduced to the form of Reynolds Averaged Navier-Stokes (RANS) Equations in CFD tools of ANSYS software. These are the time-averaged equations of motion with respect to the fluid flow. The RANS equations were approximated in this paper using k-ω SST turbulence model.

Using periodic boundary condition, the simulation of air flow through one blade was extrapolated to the other two blades so that the values on the three blades of the rotor section were visually observed.

When performing any simulation problem, meshing is also a very important job because it greatly affects the accuracy of the solution as well as the convergence of the problem. In addition, the meshing at the boundary layers also needs to be paid attention, because when

performing calculations with air flow passing through turbine blade, the separation of air flow on blade surface affects the pressure distribution on the blade surface.

For accurate calculation results, the boundary layer near the blade surface is usually more finely divided and is a structured mesh. The computational domain and meshing of the CFD problem in this paper were shown in Fig. 2. The number of elements and the number of mesh nodes of the model were 1,142,937 and 1,840,945 respectively.

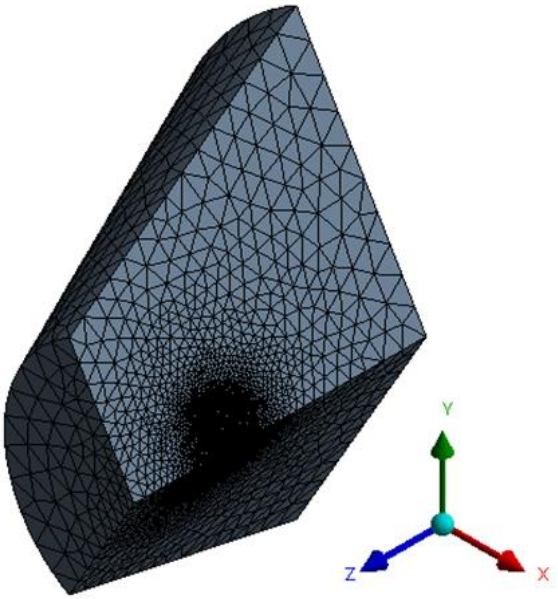

a. Computational domain and meshing grid

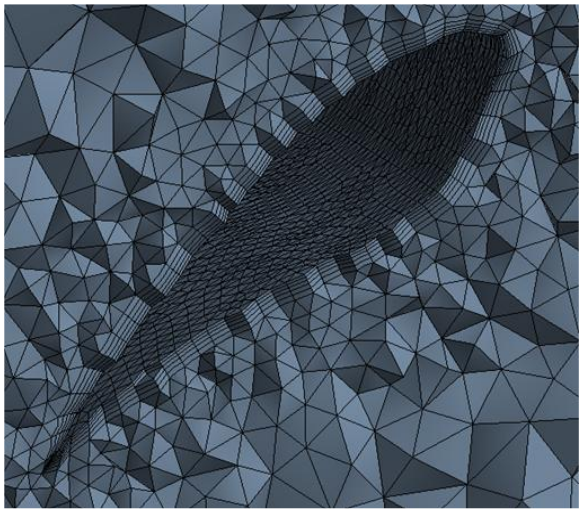

b. Meshing grid near turbine blade

Fig. 2. Calculational domain and meshing grid in CFD problem

In this simulation research, Skewness and Orthogonal Quality values were used to assess the mesh quality. For the generated mesh, the Orthogonal Quality is greater than 0.25 and Skewness is less than 0.75. Based on the criteria outlined in Table 4 by ANSYS [16], this mesh was considered to have good quality.

Table 4. Mesh Quality Assessment

Quality	Skewness	Orthogonal
Inappropriate	0.98-1.00	0-0.01
Bad	0.95-0.98	0.001-0.15
Sufficient	0.80-0.95	0.15-0.20
Good	0.50-0.80	0.20-0.70
Very Good	0.25-0.50	0.70-0.95
Outstanding	0-0.25	0.95-1.00

CFD analysis showed the pressure distribution across the blade surface. From the output parameters, the value of the torque could be also calculated. Air flow through turbine blades was considered at standard conditions of 15 degree Celsius.

2.3. Fluid-Structure Interaction Setup

In FSI model, the result of the pressure distribution on the blade surface from CFD problem was considered as the input pressure loading condition. From there, the results of stress and deformation on the blade was determined.

In FSI problem, turbine blade was determined to consist of two components such as outer blade surface and inner supporting beam (Fig. 3a) for details.

The thickness of the outer surface of the blade decreased linearly from 0.1 m at the root to 0.005 m at the tip. Similarly, the thickness of the supporting beams also decreased linearly from 0.1 m at the part closest to the root to 0.03 m at the tip. This blade thickness corresponded to positions along the X-direction in the global coordinate system.

Besides aerodynamic loads, there were two other important forces acting on the blades: gravity and centrifugal force (which causes the rotation of the blades). Thus, the loads applicable to the FSI problem included the aerodynamic load from the CFD problem, the rotor rotational speed to account for the centrifugal force, and the gravitational force. In addition, a fixed boundary condition is also applied to the root of the blade. The blade was divided into a structured mesh (Fig. 3b).

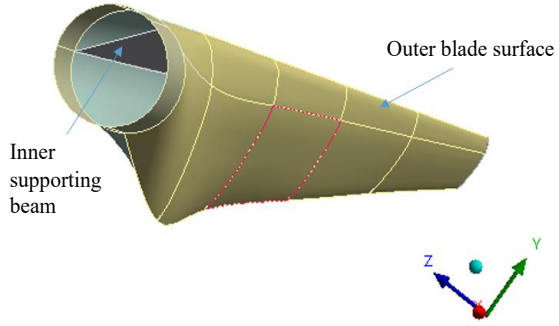

a. Computational domain and meshing grid

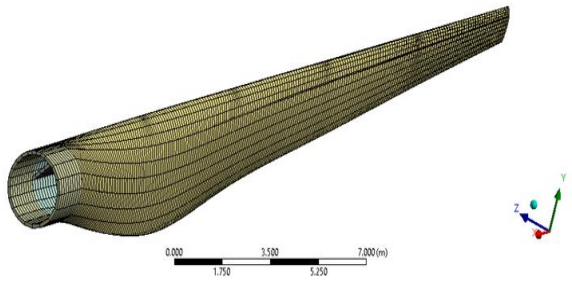

b. Meshing grid near turbine blade

Fig. 3. Calculational domain and meshing grid in FSI problem

3. Results

3.1. Computational Fluid Dynamics Results

To evaluate the results of the CFD problem, the mass flow rate results was firstly examined. The result at inlet and outlet was approximately the same (Table 5), it could be concluded that the simulation results were relatively accurate.

Table 5. Mass flow rate results

Mass flow rate	[kg/s]
Inlet	146871.08
Inlet-top	442917.75
Outlet	-589788.83
Net	-0.0045713602

The theoretical wind speed at the blade tip depended on the diameter of rotor, including blade length 43.2 m and 1 m in the direction of the blade length from the root to the hub rotor, and the angular velocity 2.22 rad/s. The velocity at the tip of the blade was 98.12 m/s. Comparing the results of this theoretical calculation with the simulation results performed by ANSYS software in Fig. 4a, the simulation results and the theoretical results gave different results of 0.016%. These results also approximated with the value provided by the manufacturer of 97 m/s [13]. In addition, streamlines of air flow were shown in Fig. 4b.

The result of velocity vector on the *YZ* plane at the position 15 m in the *X* direction from the root of the blade was shown in Fig. 4c.

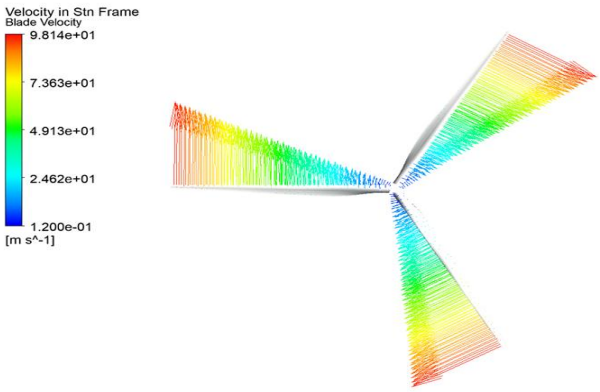

a. Velocity vector along turbine blade

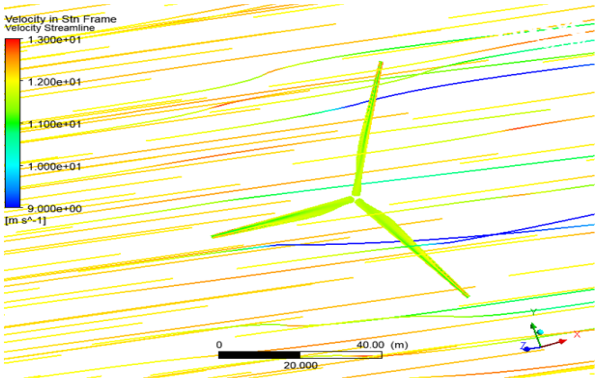

b. Streamline of air flow

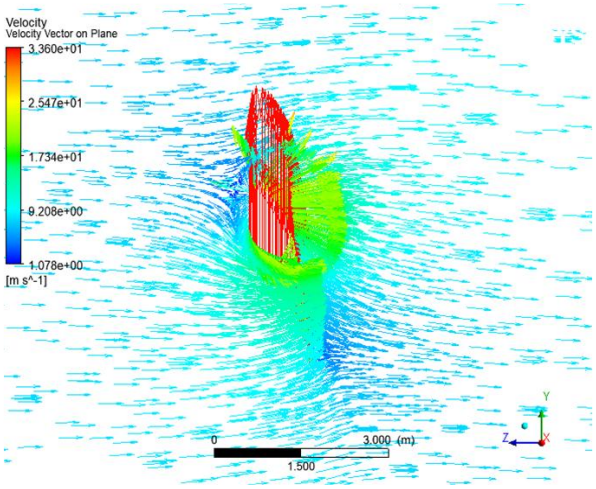

c. Velocity vector at position 15 m from root

Fig. 4. Velocity vector and streamline

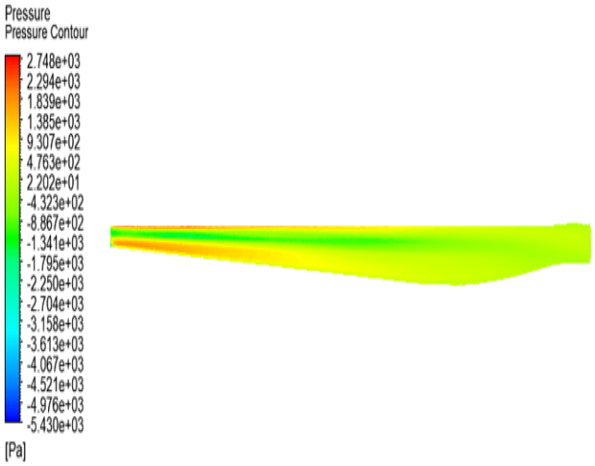

a. Pressure on face-surface of blade

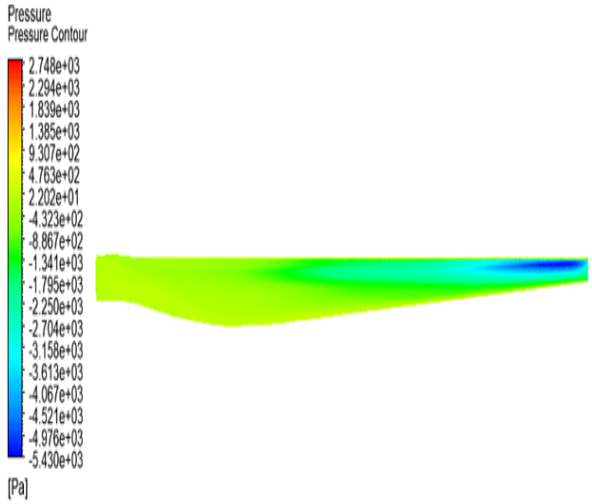

b. Pressure on back-surface of blade

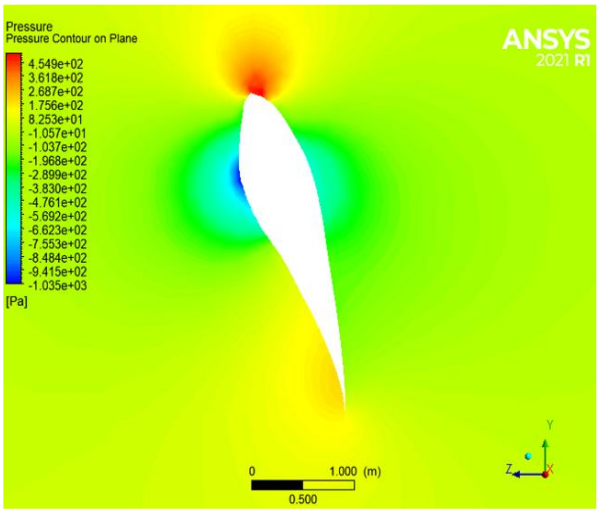

c. At position 15 m from root

Fig. 5. Distribution of pressure

The results of the pressure distribution on face and back surfaces of turbine blades were shown in Fig. 5a and Fig. 5b. Obviously, maximum pressure on face surface (face that directly collided with the air inlet) of the turbine blade. And face-surface pressure was greater than back-surface pressure.

For more detail, results of pressure distributions over a plane were considered at *YZ* plane with the *X*-direction 15 m from the root of the blade (Fig. 5c). Pressure was maximum at stagnation point where air and blade were first met and was minimum at maximum thickness of airfoil.

3.2. Fluid-Structure Interaction Results

To evaluate the results of FSI problem, the theoretical centrifugal force was firstly compared with simulation result. Centrifugal force was a radial force that depended on mass and radial acceleration. It had a value equal to the value of reaction force at the root of the blade, where it was attached to rotor hub. The formula for calculating centrifugal force was determined as following:

$$F_r = m * r * \omega^2 \quad (1)$$

where, m is total mass of the blade and r is the distance in the radial direction where the mass was applied. In this case, r lies at the centre of the blade in radial direction. And ω is angular velocity.

The blade mass and blade centre of gravity were determined using ANSYS Mechanical tools. The mass of the blade in this case was 23,538 kg and the centre of gravity of the blade had coordinates (-14.23, -0.2085, 0.16236). Thus, centrifugal force was 1,580,100 N. The result calculated by ANSYS Mechanical software differed by 0.234% with theoretical results. Therefore, calculation results in FSI problem had high accuracy.

Von-Mises equivalent stress (Fig. 6) was determined under the influence of pressure load distributed on the blade as shown in Fig. 5a and Fig. 5b for the face and back surface of the blade, respectively. The maximum value of the equivalent stress in this case reached maximum value of 42.875 MPa and minimum value of approximately 0.086 MPa. The greatest stress was concentrated in the proximal half of the blade. The maximum stress value was much smaller than critical value of material in Table 3. Thus, the blade was concluded to be over-strong.

Total deformation of the blades had an important quantity to evaluate the effect of aerodynamic elasticity on the blades. In this case, it was because of the effect of pressure load distribution on the blade surface. Total deformation was determined in Fig. 7. The result of maximum total deformation of the blade was 0.627 m and occurred at the tip of the blade, where thickness was the smallest.

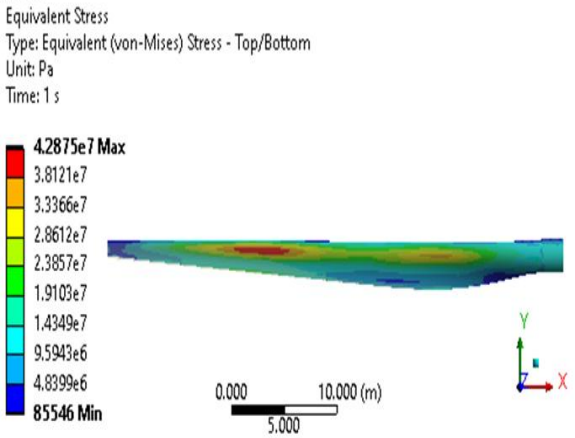

a. On face-surface of blade

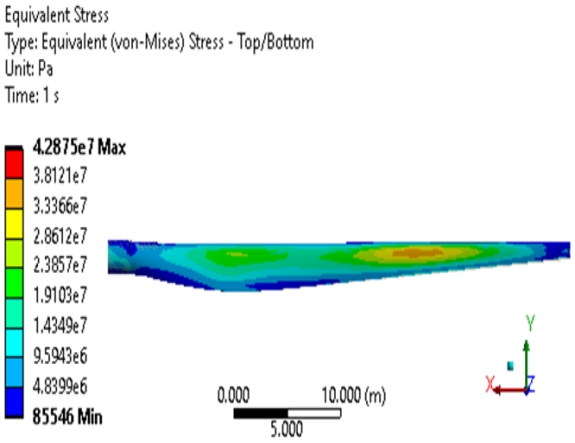

b. On back-surface of blade

Fig. 6. Distribution of equivalent stress

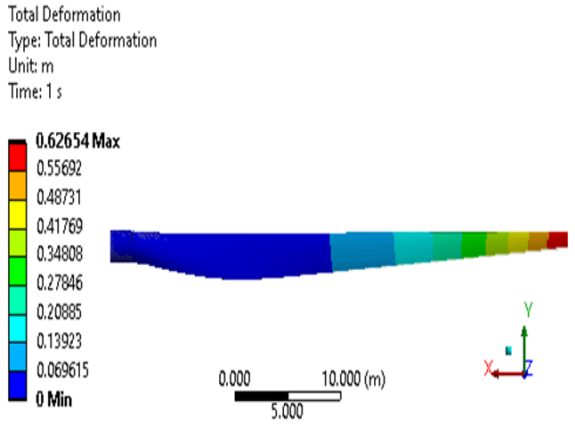

Fig. 7. Results of total deformation

4. Conclusion

GE1.5XLE turbine blade of HAWT wind turbines was studied in this paper with help of CFD and FSI tool in ANSYS software. Both CFD and one-way FSI problem was in good accord with theorical result and data of manufacturer within less 2% of relative error.

Velocity along turbine blade increased with the distance from the root to the tip. The maximum velocity value was obtained at the tip of the blade. The pressure on face-surface of the blade was greater than that on back-surface. The maximum pressure was found at stagnation position, where the air and the blade first met.

With an inlet air velocity of 12 m/s, maximum deformation of the blade was 0.627 m at the tip, where thickness is the smallest. Meanwhile, maximum stress reached 42.875 MPa in the proximal half of the blade. The blade was concluded to be too durable within considered working limits.

In the future, this research will focus on the influence of materials as well as determining the natural frequencies of the blades. In addition, two-ways FSI problem will be also mentioned to determine the actual phenomena occurring on the wind turbine.

Acknowledgments

The authors would like to thank to ANSYS, Inc. for the authorization of using ANSYS software in simulation works.

References

[1] P. S. Veers, T. D. Ashwill, H. J. Sutherland, D. L. Laird, D. W. Lobitz, D. A. Griffin, J. F. Mandell, W. D. Musial, K. Jackson, M. Zuteck, A. Miravete, S. W. Tsai, and J. L. Richmond, Trends in the design, manufacture and evaluation of wind turbine blades, Wind Energy: An International Journal for Progress and Applications in Wind Power Conversion Technology, vol. 6, iss. 3, pp. 245–259, Jun. 2003. https://doi.org/10.1002/we.90

[2] R. L. Bisplinghoff, H. Ashley, and R. L. Halfman, Aeroelasticity, New York, NY, USA: Dover Publications, 1996.

[3] C. A. Dahl, Renewable resources for electric power: Prospects and challenges, Resources Policy, vol. 27, iss. 1, pp. 59–60, Mar. 2001. https://doi.org/10.1016/S0301-4207(00)00046-5

[4] P. D. Fleming and S. D. Probert, The evolution of wind-turbines: An historical review, Applied Energy, vol. 18, iss. 3, pp. 163–177, 1984. https://doi.org/10.1016/0306-2619(84)90007-2

[5] I. Dincer and M.F. Ezzat, 3.4 Renewable energy production, Comprehensive Energy Systems, pp. 126–207, 2018.

[6] J. E. Withee, Fully coupled dynamic analysis of a floating wind turbine system, PhD dissertation, Massachusetts Institute of Technology (MIT), Cambridge, MA, USA, 2004. [Online]. Available: http://hdl.handle.net/1721.1/43619

[7] M. H. H. Albadi, On techno-economic evaluation of wind-based distributed generation, PhD dissertation, University of Waterloo, Waterloo, ON, Canada, 2010.

[8] VISCWIND project, Viscous effects on wind turbine blades, Technical Report, ET-AFM-9902, JOULE III Project (JOR3-CT95-0007), Technical University of Denmark, Denmark, 1999.

[9] M. H. Hansen, Vibrations of a three-bladed wind turbine rotor due to classical flutter, Proceedings of the ASME 2002 Wind Energy Symposium, ASME 2002 Wind Energy Symposium, Reno, Nevada, USA, pp. 256–266, Jan. 2002. https://doi.org/10.1115/WIND2002-48

[10] N. A. Mezaal, K.V. Osintsev, and S.V. Alyukov, The computational fluid dynamics performance analysis of horizontal axis wind turbine, International Journal of Power Electronics and Drive Systems, vol. 10, no. 2, pp. 1072–1080, Mar. 2019. http://doi.org/10.11591/ijpeds.v10.i2.pp1072-1080

[11] L. Wang, R. Quant, and A. Kolios, Fluid structure interaction modelling of horizontal-axis wind turbine blades based on CFD and FEA, Journal of Wind Engineering and Industrial Aerodynamics, vol. 158, pp. 11–25, Nov. 2016. https://doi.org/10.1016/j.jweia.2016.09.006

[12] E. M. Shamso, A. El-Megharbel, S. Elsanabary, R. Soliman, and M. Elhadek, Modeling and response of horizontal axis wind turbine blade based on fluid-structure interaction, Port-Said Engineering Research Journal, Oct. 2023. https://doi.org/10.21608/pserj.2023.239660.1266

[13] M. Sakala, M. Suzuki, and K. Ameku, Computational Fluid Dynamics Analysis of Horizontal Axis Wind Turbines Performance Grand Renewable Energy 2018 Proceedings, O-We-7-1, Yokohama, Japan, Jun. 2018.

[14] N. J. Vermeer, Performance measurements on a rotor model with Mie-vanes in the Delft Open Jet Tunnel, IW-91048R, Institute for Wind Energy, Delft University of Technology, 1991.

[15] N. A. Mamaghani and P. E. Jenkins, Computational fluid dynamics analysis of multi-bladed horizontal axis wind turbine rotor, World Journal of Mechanics, vol. 10, no. 9, pp. 121–138, Sep. 2020. https://doi.org/10.4236/wjm.2020.109009

[16] ANSYS, Inc., ANSYS Mesh Metrics Explained, ANSYS Help Documentation, Canonsburg, PA, USA: ANSYS, Inc.